Available online at www.sciencedirect.com
ScienceDirect
Journal of Nuclear Materials 375 (2008) 135–143
journal of nuclear materials
www.elsevier.com/locate/jnucmat

An exploratory study to determine applicability of nano-hardness and micro-compression measurements for yield stress estimation

P. Hosemann [a,b,*], J.G. Swadener [a], D. Kiener [d], G.S. Was [c], S.A. Maloy [a], N. Li [a]

[a] Los Alamos National Laboratory, P.O. Box 1663, Los Alamos, NM 87544, USA
[b] Montanuniversität Leoben, Franz-Josef-Strasse 18, 8700 Leoben, Austria
[c] University of Michigan, 2300 Hayward St Ann Arbor, MI 48109-2136, USA
[d] Austrian Academy of Science, Jahnstrasse 12, 8700 Leoben, Austria

Received 22 October 2007; accepted 28 November 2007

Abstract

The superior properties of ferritic/martensitic steels in a radiation environment (low swelling, low activation under irradiation and good corrosion resistance) make them good candidates for structural parts in future reactors and spallation sources. While it cannot substitute for true reactor experiments, irradiation by charged particles from accelerators can reduce the number of reactor experiments and support fundamental research for a better understanding of radiation effects in materials. Based on the nature of low energy accelerator experiments, only a small volume of material can be uniformly irradiated. Micro and nanoscale post irradiation tests thus have to be performed. We show here that nanoindentation and micro-compression testing on T91 and HT-9 stainless steel before and after ion irradiation are useful methods to evaluate the radiation induced hardening.

1. Introduction

Ferritic/martensitic stainless steels are the primary candidate materials for high dose nuclear applications. Their low swelling, low activation, resistance to embrittlement and hardening, and corrosion resistance make them well suited for use in nuclear reactors and spallation targets [1]. To investigate the materials behavior under irradiation, mechanical tests on ferritic/martensitic steels irradiated in reactors or spallation sources have been performed in the past [2,3]. Due to the fact that the specimens are usually highly radioactive, these tests had to be performed in hot cells and in radiation controlled facilities. This raises the costs and increases the time needed to perform the tests. Moreover, the dose rate, the environment and temperature range are usually very limited in such experiments. A low energy proton beam can be used to induce radiation damages in the material [4,5] and investigate radiation effects in materials without highly activating the specimens which leads to significantly reduce the costs. Due to the low energy of the protons, however, the proton penetration depth is limited. Therefore, new methods of testing the irradiated materials need to be developed. Nanoindentation [6], micro-compression testing [7] and scanning electron microscopy (SEM) are small scale methods which can be applied to investigate the changes of microstructure and mechanical properties due to irradiation in small volumes. In the presented work, we applied these mentioned methods to investigate the changes in the mechanical properties due to proton irradiation.

2. Experiment

2.1. Irradiation

Two samples of each material (Sandvik HT-9 and X10CrMoVNb 9-1 (Modified 9Cr1Mo or also known as

* Corresponding author. Address: Los Alamos National Laboratory, P.O. Box 1663, Los Alamos, NM 87544, USA. Tel.: +1 505 629 9893; fax: +1 505 667 7443.
E-mail address: peterh@lanl.gov (P. Hosemann).

0022-3115/$ - see front matter © 2007 Elsevier B.V. All rights reserved.
doi:10.1016/j.jnucmat.2007.11.004

Table 1
The nominal composition in wt% of the tested alloys

Material	Fe	Cr	Mo	Si	C	Mn
T91	Balance	9.3	0.95	0.43	0.1	–
HT-9	Balance	11.95	1.0	0.4	0.2	0.6

grade 91)) were implanted with 2.3 MeV He^+ at room temperature using the Tandetron Accelerator in the Michigan Ion Beam Materials Laboratory at the University of Michigan. The nominal composition of the tested materials is given in Table 1. The samples were rotated from 0° to 70° in 5° increments in order to achieve a uniform He distribution [4]. The number of He ions incident on the samples for each angle was also monitored using a beam current integrator. The helium concentration was uniform at ~100 appm over the depth range between 1 μm and 4 μm (see Fig. 1). Four samples of each material (two with He implantation and two without He implantation) were irradiated using 2 MeV protons at a dose rate of approximately 2×10^{-5} dpa/s (the doses and dose rates are calculated with the SRIM2003 [8] simulation). The proton irradiations were performed using the General Ionex Tandetron accelerator at the Michigan Ion Beam Materials Laboratory at a temperature of 450 °C ± 5 °C. This resulted in a nearly uniform amount of damage through the first 15 μm of the total proton range of 20 μm. The resulting damage caused by the proton irradiation was 3 dpa (samples HT-9-3dpa, HT-9-3dpa+He and samples T91-3dpa and T91-3dpa+He) and 7 dpa (samples HT-9-7dpa, HT-9-7dpa+He and samples T91-7dpa, T91-7dpa+He) for each material. The irradiation stage was designed to control the sample temperature by controlling the stage temperature. The copper stage was heated using a resistive cartridge heater and cooled using room temperature air flowing through cooling lines that penetrate the back of the stage. Three to five type J (iron/constantan) thermocouples (spot welded directly to the sample surfaces to provide point temperature measurement) and a calibrated infrared pyrometer was used to monitor the sample temperature during irradiation. The irradiation stage was

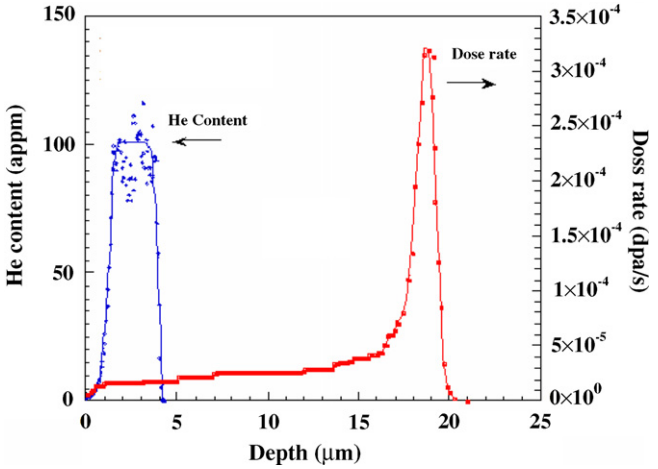

Fig. 1. Dose rate depth profile calculated using SRIM 2003 [7].

electrically isolated from the beam line and grounded. Four rectangular tantalum apertures were used to define the irradiation area on the samples (10 mm in height 18 mm in width). The approximately 3 mm diameter proton beam was raster-scanned across the stage so that about half the total beam current was deposited on the samples and half on the apertures to ensure that samples at any position on the stage receive the same dose. The beam current was extremely stable during the irradiation, with up to 75 μA on the samples at times.

2.2. Post irradiation testing

2.2.1. Nanoindentation in cross-section

After irradiation, the samples were cut in half using a slow speed cutting saw. One half of the sample was used to perform pre-corrosion analysis (nanoindentation and micro-compression testing in cross-section), while the other half was used for corrosion testing in liquid lead bismuth eutectic. The pre-corrosion test sample was mounted in epoxy cold mount and polished with 0.1 μm colloidal silica as the last step on a Buehler vibromet polisher. This provided a very flat and smooth surface as required for nanoindentation. The nanoindenter used was a Hysitron Triboindenter® instrument equipped with a multi-range nanoprobe, an optical microscope and an atomic force microscope (AFM). A Berkovich diamond indenter tip was used to perform the nanoindentation measurements. Starting from the edge, 10 rows with 10 indents in each row were placed parallel to the edge. This provided 10 indents at the same distance from the edge. The indents were 4 μm apart from each other, resulting in a 36 μm × 36 μm array of 100 indents for each specimen condition (see Figs. 2(a) and 3). Constant displacement mode was used for all indents to ensure constant indentation depth. This eliminates the influence of the indentation size effect [9] within one array of indents. Before and after performing the array of indents, a contact mode AFM image using the indenter tip was scanned to ensure the location of the indents. In order to compare these results to micro-hardness data and also to properties like yield strength, it is necessary to take the indentation size effect into account [6,9,10]. Therefore, indentation depth vs. hardness curves for the un-irradiated materials were obtained. This was done using the high load Hysitron indentation head which allows a maximum force of 2 N. A Berkovich indenter tip was used to perform indents up to a depth of 3 μm in an un-irradiated area of the sample. Seven different indentation depths (200 nm, 300 nm, 450 nm, 675 nm, 1500 nm, 2250 nm, and 3000 nm) and 7 indents of each depth were performed. The resultant curve (hardness vs. depth) was then used with the Nix and Gao [10] model in order to extrapolate the nano-hardness data to micro-hardness.

2.2.2. Micro-compression testing

After the nanoindentation tests were performed on all specimens, HT-9 (7dpa+He) was selected for micro-com-

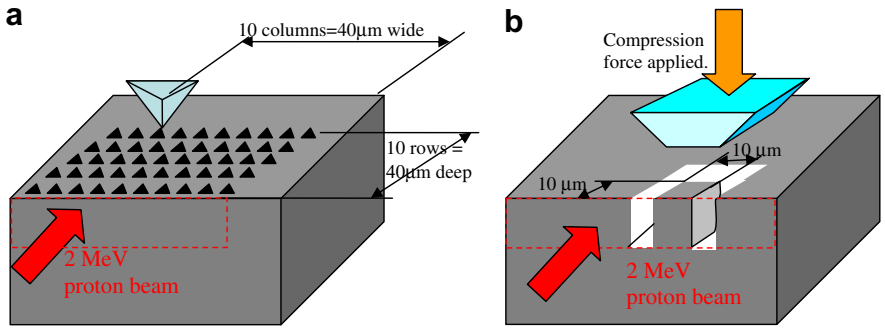

Fig. 2. Schematic sketch of the nanoindentation measurements (a). Schematic sketch of the pillar testing measurements (b).

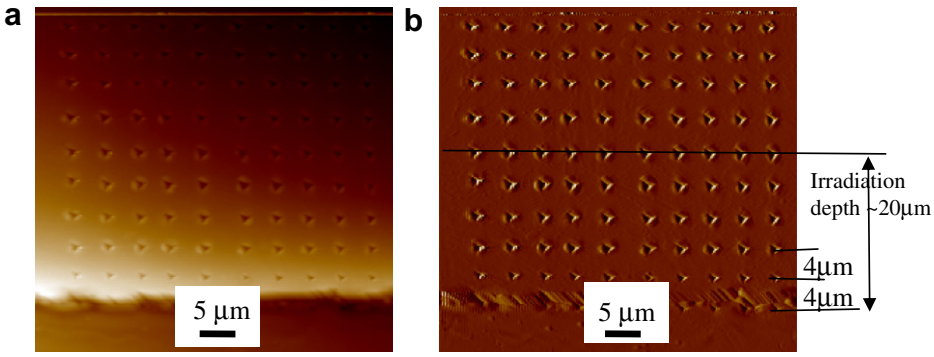

Fig. 3. 50 μm × 50 μm AFM scan on HT-9-3 dpa with the array of 100 indents. (a) The topography image and (b) the gradient image. Implantation depth are indicated.

pression tests. These were performed at the Montanuniversität Leoben, Austria, using a dual beam focussed ion beam (FIB) workstation (Zeiss LEO 1540 XB). A preform for the final column, having a square cross-section with a side length $a = 8$ μm and a height $h = 15$ μm, was FIB milled using Ga^+ ions with a kinetic energy of 30 keV under perpendicular ion impact, using an ion current of 2 nA. A slight taper of the side planes is an unavoidable artefact of this milling setup [7]. Consequently, in a second step, the shape of the columns was finalized to a side length of $a = 5$ μm and a height of $h = 10$ μm using grazing ion impact with a reduced milling current of 100 pA (see Fig. 4). The two samples on the irradiated side were placed close to the nanoindentation array. The centre of each sample was ~10 μm behind the irradiated sample surface, and in the centre of a single large grain. The samples on the un-irradiated side were placed well behind the edge. The grain boundaries and martensite lamella were identified using channelling contrast, and the exact column dimensions and position were identified in the SEM after accomplishing FIB shaping.

The sample loading was performed in situ using a micro-indenter (ASMEC, UNAT) equipped with a flat diamond tip mounted in a SEM (LEO Stereoscan 440). This allows

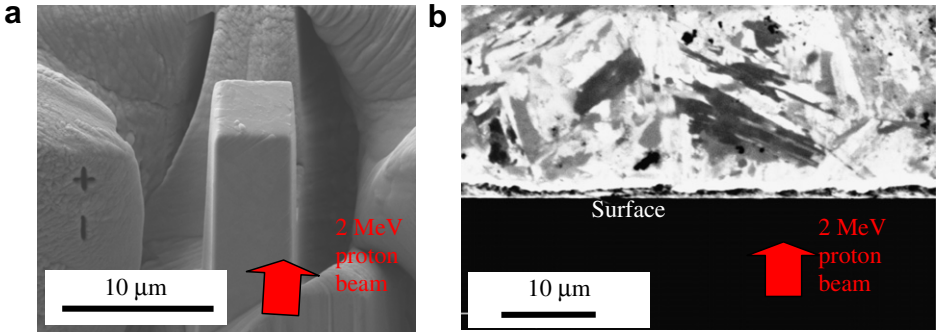

Fig. 4. (a) SEM image presenting the columns for micro-compression testing machined by FIB milling on the irradiated area of sample HT-9-7dpa+He. (b) Secondary ion image using the FIB on the micro-compression testing area.

a very precise alignment between sample and punch as well as the possibility to directly monitor the ongoing deformation. The compression tests were conducted open loop in displacement controlled mode to ensure a compression of all samples to strains larger than 15% [11].

3. Results

3.1. Nanoindentation

The results from the nanoindentation tests are presented in Figs. 5 and 6. They show an increase in hardness due to the irradiation. The amount of increase depends on the irradiation dose (3 dpa or 7 dpa). With cross-section nanoindentation, the effect of He implantation could not be detected, because the implanted layer was too thin. Moreover, no significant hardness increase due to the beam stopping peak at a depth of ~18 μm was found. For comparison,

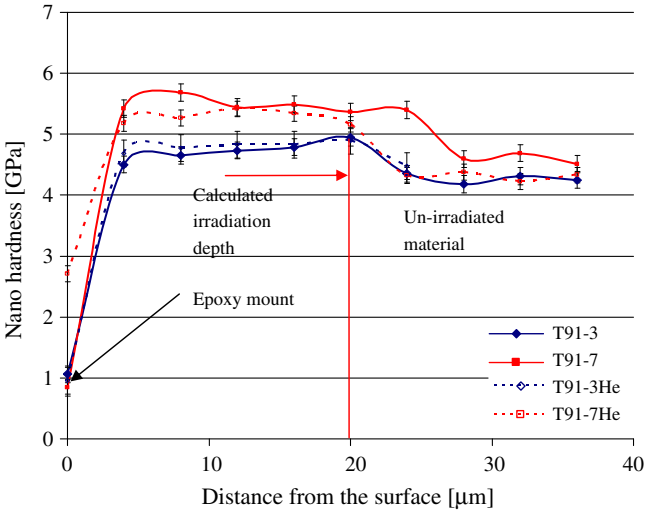

Fig. 5. Depth dependant nano-hardness measurements for T91.

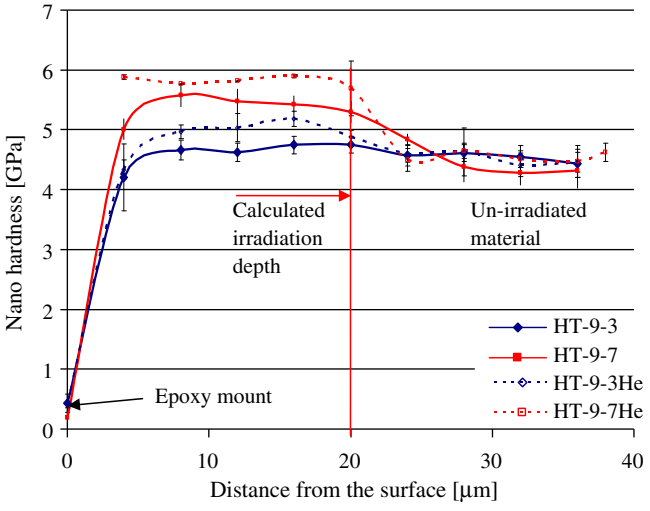

Fig. 6. The nano-hardness vs. depth measurements for HT-9.

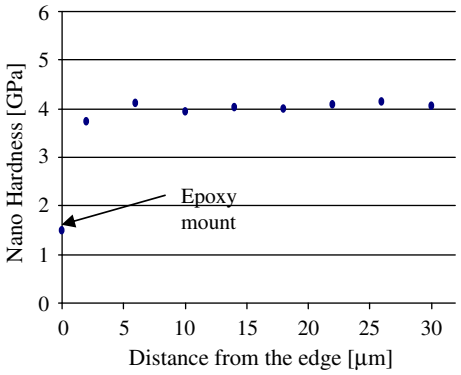

Fig. 7. Nanoindentation measurements on the un-irradiated side of the sample HT-9-7dpa.

the same measurement was performed on the un-irradiated side of the sample. Fig. 7 shows results obtained for the un-irradiated side of the sample HT-9-7dpa. No increase in hardness at the edge area was observed. The hardness vs. indentation depth measurements in non-irradiated areas of these samples using the high load head reveal a strong indentation size effect. Fig. 8 shows that at an indentation depth of ~3 μm (~15 μm lateral size), the hardness does vary only slightly with depth and is ~3 GPa (~306 kg/mm^2) which is similar to results gained from a Vickers micro-hardness measurement (290 kg/mm^2) performed using a Boehler MicroMet® 5100, and values found in the literature (280–300 kg/mm^2 [12,13]).

3.2. Micro-compression testing

The collected force–displacement data were converted to stress–strain curves using the sample dimensions measured prior to deformation. In addition to compression of the columns themselves, they were also punched into the base material. This problem was analytically solved by Sneddon [14] for a rigid flat punch penetrating an infinite half-space and applied to the initial force–displacement data as suggested by Volkert and Lilleodden [15]. Fig. 9 shows the true stress–strain data for the two columns on the irradiated side and Fig. 10 for the un-irradiated side.

4. Discussion

Figs. 5 and 6 show that the radiation hardened areas can accurately be measured using nanoindentation. At 20 μm depth, a sudden hardness drop (ΔH_n) is found between 0.12 GPa–1.26 GPa for T91 and HT-9, depending on the sample and dose. Each data point in these figures represents the average hardness value over 10 indentations. The averaged percentage hardness increase (compared to the un-irradiated area) is given in Table 2. It can be seen that the hardness increase in HT-9 due to irradiation is slightly higher than that in T91. This might be due to the fact that HT-9 has a 3 wt% higher Cr content than T91 and therefore more α′-phase can be formed during irradiation. Also more local radiation induced segregation is possible.

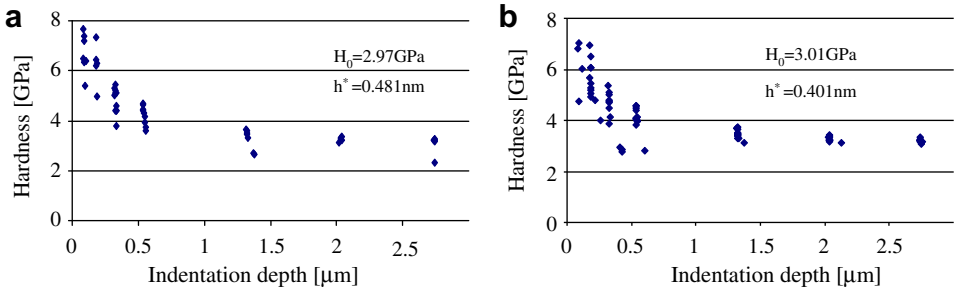

Fig. 8. Hardness vs. indentation depth of (a) HT-9 and (b) T91. These data are used to determine H_0 and h^* for using the Nix and Gao model [9].

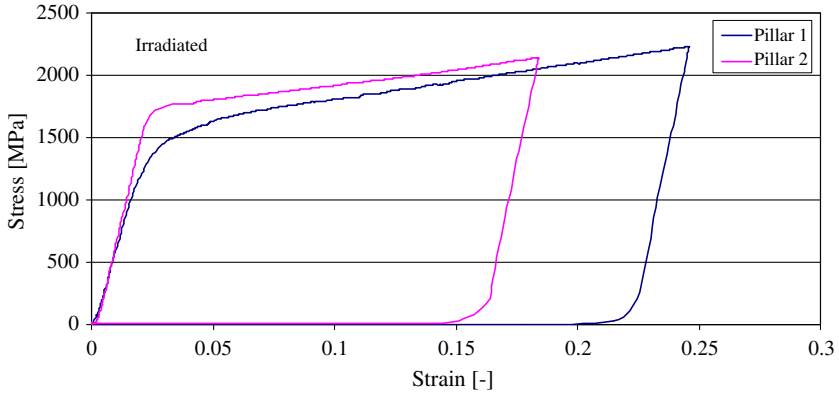

Fig. 9. True stress–strain curve for 2 micro-compression tests performed on HT-9-7dpa+He at the irradiated area.

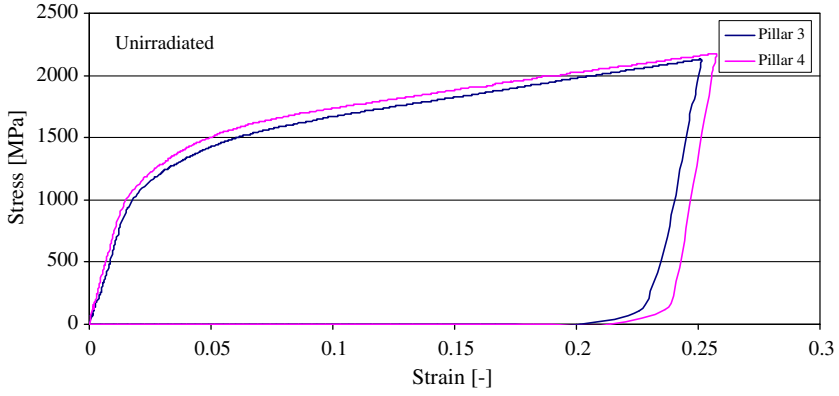

Fig. 10. True stress–strain curve for 2 micro-compression tests performed on HT-9-7dpa+He at the un-irradiated area.

The data obtained through nanoindentation cannot be compared directly with micro-hardness data. The indentation size effect [6,9,10], which can be described using the geometrically necessary dislocation theory, does lead to higher values for smaller indents. According to [10], as long as the indent size is >50 nm, the Nix and Gao model can be used to describe the nanoindentation size effect and calculate micro-hardness values for indents deeper than 2 μm. To apply this model, the hardness vs. indentation depth curve must be measured for each material. The corresponding curves can be seen in Fig. 8. Using the hardness vs. indentation depth curve, the constants H_0 and h^* required for the Nix and Gao model,

$$H_0/H = H/(1 + h^*/h)^{0.5}, \tag{1}$$

can be calculated. h^* is used to calculate H_m (micro-hardness) for every point in the hardness vs. location curve in Figs. 11(a) and 12(a). The R^2 values for these fits are 0.83 for both HT-9 and T91.

In order to calculate the yield stress, the correlation proposed by Busby et al. [12] is applied. Experimental data gained from tensile tests and micro-hardness tests showed that

$$\sigma_y = 3.06H_v, \tag{2}$$

where H_v is Vickers hardness and σ_y is yield strength.

Table 2
Measured and calculated values using the hardness data

Material	H_n^* (GPa)	S.D.	H_n (GPa)	S.D.	ΔH_n (GPA)	S.D.	$\Delta H_m^\dagger$ (GPa)	S.D.	$\sigma_y^{\dagger *}$ (MPa)	Dev.	$\sigma_y^\dagger$ (MPa)	Dev.	$\Delta\sigma_y^\dagger$ (MPa)	Dev.
HT9-3dpa	4.69	0.06	4.54	0.09	0.15	0.15	0.08	0.07	742	10	716	4	25.5	14
HT9-7dpa	5.27	0.05	4.33	0.11	0.94	0.16	0.54	0.08	860	35	684	40	176.2	75
HT9-3dpa+He	5.01	0.11	4.53	0.13	0.48	0.24	0.25	0.12	792	18	711	17	80.8	35
HT9-7dpa+He	5.81	0.09	4.55	0.08	1.26	0.17	0.46	0.08	865	10	716	13	148.9	22
T91-3dpa	4.72	0.08	4.27	0.12	0.45	0.2	0.31	0.11	901	24	800	14	101	38
T91-7dpa	5.47	0.08	4.60	0.11	0.87	0.19	0.52	0.12	1035	22	866	17	167	39
T91-3dpa+He	4.80	0.07	4.68	0[a]	0.12[a]	0.07[a]	0.2	0.02[a]	911	15	843	0[a]	67	15[a]
T91-7dpa+He	5.27	0.07	4.31	0.11	0.96	0.18	0.57	0.1	998	19	812	12	186	31

H_n^* – Averaged hardness measured with the nanoindenter at the irradiated area.
H_n – Averaged hardness measured with the nanoindenter at the un-irradiated area.
$\Delta H_n - H_n^* - H_n$.
ΔH_m – Micro-hardness increase due to irradiation calculated from ΔH_n using the NIX, Gao model.
$\sigma_y^{\dagger *}$ – Yield stress at the irradiated area using $H_m^\dagger$ and applying [9] to it.
$\sigma_y^\dagger$ – Yield stress at the un-irradiated area using $H_m^\dagger$ and applying [9] to it.
$\Delta\sigma_y - \sigma_y^{\dagger *} - \sigma_y^\dagger$.
Dev. – $1/n\sum(x-\bar{x})$.
[a] Only one value measured.

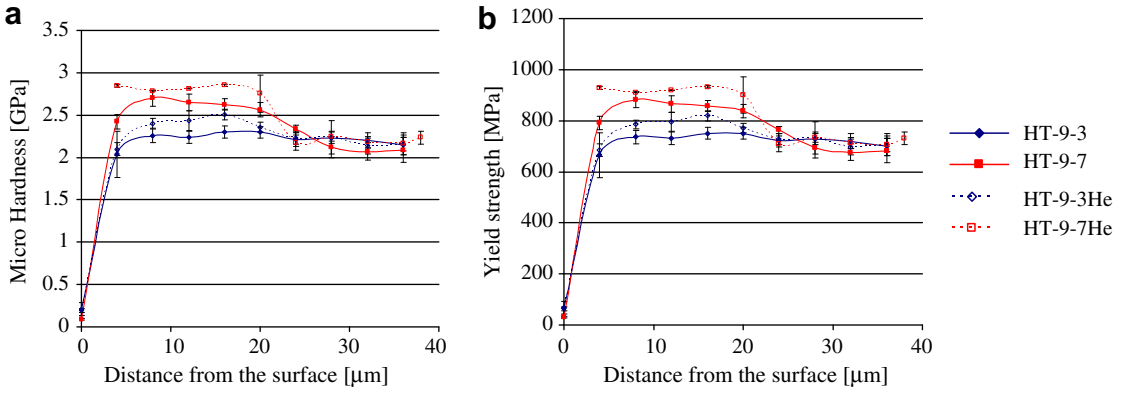

Fig. 11. (a) The macroscopic hardness calculated on HT-9 using the Nix and Gao model, and (b) the corresponding yield stress, using the conversion factor from Busby [11].

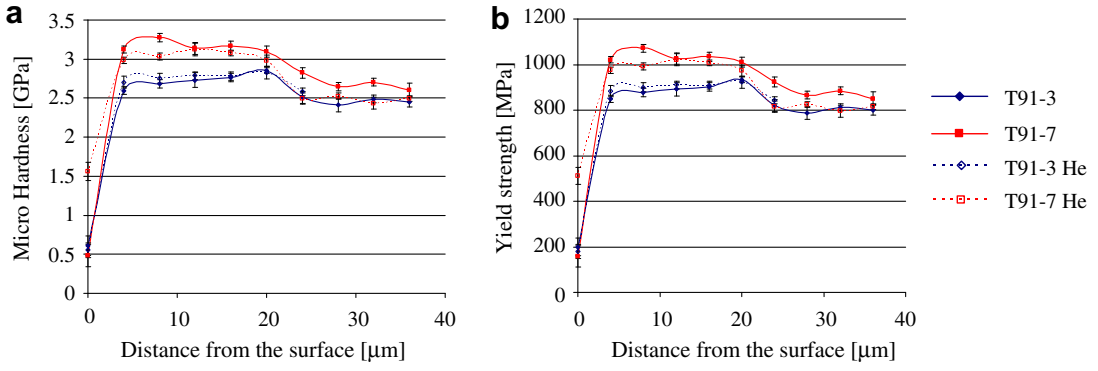

Fig. 12. The macroscopic (>3 μm deep) hardness calculated on T91 using the Nix and Gao model (a) and the corresponding yield stress using the conversion factor from Busby [11] (b).

The calculated yield stress data are shown in Figs. 11(b) and 12(b). The yield strength increase (irradiated vs. non-irradiated) is presented in detail in Table 2. These calculations give yield stress values in the range of ~700 MPa for HT-9 and ~800 MPa for T91. These values are higher than measured in macroscopic tensile tests performed on the

same heat of material (677–682 MPa for T91 [16] and 620–633 MPa for HT-9 [17]). We believe that the difference in the absolute values of σ_y (nanoindentation and tensile test data) is based on the fact that the data gained by tensile testing averages over a large amount of grains while the nanoindentation data only tests a few martensitic laths which are strongly textured (the martensitic lath found here are 1–2 μm wide and 5–15 μm long) and oriented to each other. Factors such as different surface stress states (compared to the bulk) and lower dislocation densities near the surface can have an effect as well but since the nanoindents are relatively large (200 nm deep, ~1 μm wide), it is believed here that this does not contribute as much to the discrepancy as the micro-structure. Also Busby's factor of 3.06 is based on large scale tests (tensile, Vickers hardness) where a large volume is probed. Therefore, it seems plausible that the nanoindentation data and macroscopic tensile test data of σ_y are not in full agreement. Since the radiation defects in the material are nanoscale in size, it is likely that the relative hardness increase ($\Delta\sigma_y$) due to irradiation is the same in macro and nanoscale tests. It is known from [20–22] that ion irradiation can be compared with neutron irradiation data using the Ns invariant equation:

$$T_2 - T_1 = \frac{\left(\frac{kT_1^2}{E_m^v}\right)\ln\left(\frac{\phi_2}{\phi_1}\right)}{1 - \left(\frac{kT_1}{E_m^v}\right)\ln\left(\frac{\phi_2}{\phi_1}\right)}, \quad (3)$$

where k is the Boltzmann's constant, Φ_1 and Φ_2 are the dose rates in dpa/s at temperatures 1 and 2, T_1 is the irradiation temperature and E_m^v is the effective vacancy migration energy.

This calculation suggests that the data presented here can be compared to a 3 dpa and 7 dpa reactor irradiated material at ~360 °C. Irradiations performed at the Fast Flux Test Facility (FFTF) at 300 °C and 373 °C (tensile tests at room temperature in both cases up to 8 dpa (300 °C) and 9.8 dpa (373 °C) show a yield strength increase of 335 ± 35 MPa (337 °C) and 347 MPa (300 °C) [18], respectively. The estimated yield strength increases presented here are 176 ± 75 MPa (see Table 2). Considering the accuracy in estimating yield stress from hardness measurements, the magnitude of these calculations is in relatively good agreement.

In a paper by Dao et al. [19], a different approach for calculating yield stress from nanoindentation data is proposed. The shape of the load and unload curve gained by nanoindentation can be used and applied to the proposed dimensionless Π functions in [19] to calculate σ_y and $\sigma_{0.033}$ performing the reverse analysis algorithm. Here only $\Pi 1$ and $\Pi 2$ were used since E^* was directly obtained from the Triboscan Nanoindenter fit for the unloading curve. The necessary parameters C, dPa/dh can be obtained directly from the load vs. displacement curve.

This calculation was done for 6 indents in the irradiated area and 6 indents in the un-irradiated area of each sample.

According to [19], the calculation of $\sigma_{0.033}$ does not consider the indentation size effect and gives $\sigma_{0.033}$ and σ_y only for indents deeper than >1 μm. Therefore, the calculated $\sigma_{0.033}$ and σ_y values using the Dao model overestimate the macroscopic $\sigma_{0.033}$ measured with small indents. In order to calculate the macroscopic $\sigma_{0.033}$ measured with indents <1 μm, we propose to apply the Nix and Gao model using the h^* and H_0 defined above with the hardness vs. depth plot. We believe that the Nix and Gao model can be compared to the model by Dao et al. because it is based on the geometrically necessary dislocations to form the indent, and therefore it affects the load and unload curve the same way as it would affect the measured absolute hardness.

Table 3 presents the results of these calculations. The absolute values for $\sigma_{0.033}$ are higher than the σ_y values using the factor of 3.06 from Busby. But given the uncertainty of the data these values are comparable.

The micro-compression test results are in a similar range of the values calculated using the nanoindentation data. 0.2% offset yield stress was measured for each of the

Table 3
Calculated values using the Dao [17] model

Material	$\sigma_{0.033}{}^*$ (MPa)	Dev.	$\sigma_{0.033}$ (MPa)	Dev.	$\Delta\sigma_{0.033}$ (MPa)	Dev.	$\sigma_{0.033}{}^{\dagger *}$ (MPa)	Dev.	$\sigma_{0.033}{}^{\dagger}$ (MPa)	Dev.	$\Delta\sigma_{0.033}{}^{\dagger}$ (MPa)	Dev.
HT9-3dpa	1680	101	1702	125	−22	226	1035	62	1049	77	−14	139
HT9-7dpa	2116	317	1478	210	638	527	1304	195	911	129	393	324
HT9-3dpa He	1702	253	1595	107	107	360	1095	156	983	66	50	222
HT9-7dpa He	2178	141	1578	90	200	231	1343	87	973	56	123	143
T91-3dpa	1701	68	1416	96	285	164	981	42	817	59	164	101
T91-7dpa	2039	127	1596	81	443	207	1176	78	921	50	256	128
T91-3dpa He	1709	101	1657	94	52	195	986	62	956	58	30	120
T91-7dpa He	1944	124	1470	101	474	225	1121	76	848	63	273	139

$\sigma_{0.033}{}^*$ – Stress at a representative strain of 0.033% irradiated area.
$\sigma_{0.033}$ – Stress at a representative strain of 0.033% un-irradiated area.
$\Delta\sigma_{0.033}$ – $\sigma_{0.033}$ Stress increase due to irradiation.
$\sigma_{0.033}{}^{\dagger *}$ – Stress at a representative strain of 0.033% irradiated area, Nix Gao model applied.
$\sigma_{0.033}{}^{\dagger}$ – Stress at a representative strain of 0.033% un-irradiated area, Nix Gao model applied.
$\Delta\sigma_{0.033}{}^{\dagger}$ – Stress at a representative strain of 0.033% irradiated area, Nix Gao model applied.
Dev. – Deviation using $\ln\sum(x-\bar{x})$.

stress–strain curves. For the HT-9-7dpa material, $\sigma_{0.02} =$ 1534–1766 MPa ($\sigma_y = 1150$–1650 MPa) in the 7 dpa range area and $\sigma_{0.02} = 1326$–1403 MPa ($\sigma_y = 920$–930 MPa) in the un-irradiated area. The σ_y on one of the irradiated compression tests is significant higher than at the other tests. This might be due to the fact that only a small volume of material is tested and local differences (local segregation or different orientation of the Martensitic laths) can have a large influence. Differences between nanoindentation and micro-column testing data are not entirely understood but might be influenced by the fine structure in this material. The length scale determined in nanoindentation was $h^* < 0.5$ μm. The micro-pillars measured $5 \times 5 \times 10$ μm and still appear to exhibit increased yield strength from size effects acting at a size that is approximately an order of magnitude greater than in nanoindentation. A size effect at structures >5 μm is common in micro-pillar tests [11,15]. Since the length scales are different in micro-compression and nanoindentation tests, it is likely that different mechanisms are involved. It is possible that the Busby factor of 3.06 might not be fully applicable to nanoindentation at this small scale. A slightly smaller factor can cause a large change in resulting yield strength. The micro-column testing leads to a $\Delta\sigma_{0.02}$ of 200–250 MPa. This increase due to irradiation is slightly higher than measured and calculated using nanoindentation. Considering that only two pillars were tested in each area, and different methods with differing length scales were used to obtain the data, it can be stated that these results are in agreement with the nanoindentation data. Fig. 13 presents an overall method comparison of $\sigma_{y\,irr}$, $\sigma_{y\,un\text{-}irr}$, $\Delta\sigma_{y\,irr}$. Careful analysis of the micro-column testing results for strains higher than 0.02 shows that the slope (work hardening rate) of the irradiated vs. un-irradiated material is only slightly different. The micro-pillar testing on the irradiated side shows a work hardening rate of 2900–3120 MPa while the un-irradiated side shows a slope is 2500–2890 MPa. But again, only 2 tests were performed on each sample (un-irradiated, irradiated) and therefore this difference might not be significant. However, the data lead to the assumption that the irradiated material shows a slightly stronger work hardening rate than the un-irradiated material which could lead to much less ductility and therefore to radiation induced embrittlement. This is also in agreement with the literature [4,5] where it is stated that the radiation induced hardening can be described with the dispersed hardening model.

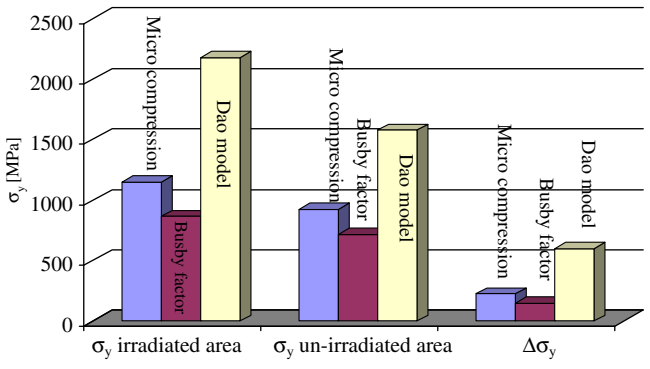

Fig. 13. Comparison of the σ_y calculations using the different methods on the sample HT-9-7dpa+He.

5. Conclusions

Based on this study on the irradiation effects on liquid metal corrosion and mechanical properties in ferritic/martensitic steels we have reached the following conclusions:

- Nanoindentation can be used to measure qualitative mechanical property changes due to ion irradiation. The location of the irradiated/un-irradiated interface can be accurately measured and agrees very well with the SRIM calculations.
- The Nix and Gao model and the Dao model can both be used to estimate a yield strength value for the irradiated area based on the nanoindentation. The resulting values are in the expected range for these materials.
- Micro-compression testing using a Focused Ion Beam and a flat head indenter can be performed on F/M steels to determine irradiation induced strength increase. These test results are in relatively good agreement with the nanoindentation values calculated using the Nix and Gao model.

Acknowledgements

This work was performed, in part, at the Center for Integrated Nanotechnologies, a US Department of Energy, Office of Basic Energy Sciences user facility. Los Alamos National Laboratory, an affirmative action equal opportunity employer, is operated by Los Alamos National Security, LLC, for the National Nuclear Security Administration of the US Department of Energy under contract DE-AC52-06NA25396. The University of Leoben, and in particular Professor Gregor Mori, was supportive of this work by allowing an extensive student exchange. Roger Johnston provided editing suggestions for this paper.

References

[1] D.S. Gelles, JNM 233 (1996) 293.
[2] Y. Dai, X. Jia, R. Thermer, D. Hamaguchi, K. Geissmann, E. Lehmann, H.P. Linder, M. James, F. Gröschel, W. Wagner, G.S. Bauer, J. Nucl. Mater. 343 (2005) 33.
[3] S.A. Maloy, T. Romero, M.R. James, Y. Dai, J. Nucl. Mater. 356 (2006) 56.
[4] G. Gupta, Z. Jiao, A.N. Ham, J.T. Busby, G.S. Was, J. Nucl. Mater. 351 (2006) 162.
[5] G.S. Was, J.T. Busby, T. Allen, E.A. Kenik, A. Jenssen, S.M. Bruemmer, J. Gan, A.D. Edwards, P.M. Scott, P.L. Andresen, J. Nucl. Mater. 300 (2002) 198.
[6] J.G. Swadener, E.P. George, G.M. Pharr, J. Mech. Phys. Solids 50 (2002) 681.
[7] M.D. Uchic, D.M. Dimiduk, J.N. Florando, W.D. Nix, Science 986 (2004) 305.

[8] J.F. Ziegler, SRIM 2003 Program, J.P. Biersack, IBM Corporation, Yorktown, NY, 2003.
[9] F. Schulz, H. Hanemann, Z. Metallkd. 33 (Heft 3) (1941).
[10] W.D. Nix, H. Gao, J. Mech. Solids 46 (3) (1998) 411.
[11] D. Kiener, C. Motz, T. Schöberl, M. Jenko, G. Dehm, Adv. Eng. Mater. 8 (2006) 1119.
[12] J.T. Busby, M.C. Hash, G.S. Was, J. Nucl. Mater. 336 (2005) 267.
[13] J.T. Busby, G.S. Was, T.R. Allen, S.A. Maloy, Proton Irradiation of Ferritic/Martensitic, Stainless Steels, Michigan Ion Beam Laboratory, Annual research report 2003.
[14] I.N. Sneddon, Int. J. Eng. Sci. 3 (1965) 47.
[15] C.A. Volkert, E.T. Lilleodden, Philos. Mag. 86 (2006) 5567.
[16] S.A. Maloy, T. Romero, M.R. James, Y. Da, J. Nucl. Mater. 356 (2006) 56.
[17] M.B. Toloczko, M.L. Hamilton, S.A. Maloy, J. Nucl. Mater. 318 (2003) 200.
[18] AFCI Materials Handbook, Rev. 5 LA-CP-06-0904.
[19] M. Dao, N. Chollacoop, K.J. Van Vliet, T.A. Venkatesh, S. Suresh, Acta Mater. 49 (2001) 3899.
[20] H. Takahashi et al., J. Nucl. Mater. 103&104 (1981) 1415.
[21] L.K. Mansur, J. Nucl. Mater. 206 (1993) 306.
[22] G.S. Was, Fundamentals of Radiation Materials Science, Springer Berlin Heidelberg, New York, ISBN 978-3-540-49471-3.